ACS APPLIED POLYMER MATERIALS

pubs.acs.org/acsapm

Article

Iodonium Borate Initiators for Cationic Photopolymerization and Their Application in Radical-Induced Cationic Frontal Polymerization

Roland Taschner, Robert Liska, and Patrick Knaack*

Cite This: *ACS Appl. Polym. Mater.* 2022, 4, 7878−7890

Read Online

ACCESS | Metrics & More | Article Recommendations | Supporting Information

ABSTRACT: Iodonium antimonates and borates are well established initiators in the field of cationic photopolymerization and preferred substances for radical-induced cationic frontal polymerization (RICFP). Extensive research in the fields of ionic liquids and lithium ion battery electrolytes made many superacids based on the borate anions available. Cyanide-ligated borane **B2** has lower molecular weight compared to state-of-the-art borates and is less expensive to synthesize from commercial starting materials. By comparing reactivity in the epoxy-based monomer bisphenol-A-diglycidylether, **B2** outperforms all commercial systems in a broad range of temperatures with excellent epoxy group conversions of up to 95%. Besides its good performance as a cationic initiator, **B2** is also capable of thermally and photochemically induced RICFP. Exceptional are transparent **B2** specimens in contrast to the tested commercial systems, which are black. High reactivity, good frontal parameters, easy synthetic access, and sufficient pot life of formulations make cyanide-ligated iodonium borates a compelling alternative to current state-of-the-art initiators.

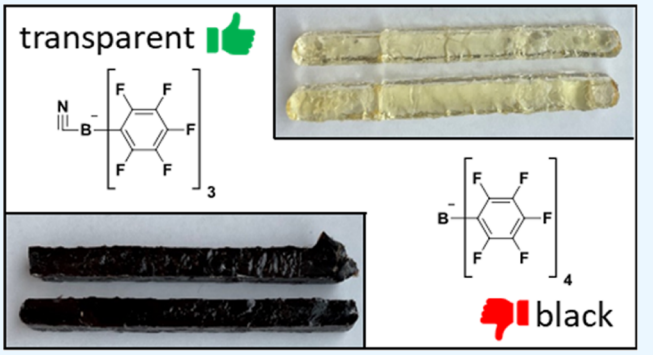

KEYWORDS: *frontal polymerization, cationic photopolymerization, iodonium borate, RICFP, TPED, BADGE*

1. INTRODUCTION

The first description of frontal polymerization (FP) was in the mid-1970s.[1−3] There, it has been described that a local reactive zone or front propagates directionally through the curable material leaving the polymerized material behind. Herewith, FP is a versatile curing tool; hence, a lot of research has been performed toward creating FPs with suitable initiators in various monomer systems.[4,5] Especially, the FP of epoxy resins is of high industrial importance as it allows the energy- and time-efficient curing of this class of materials.[6]

Photoinitiators for cationic polymerization of epoxy resins in industry mostly contain diaryliodonium and triarylsulfonium as cations. They are state-of-the-art in onium salt chemistry and efficient, stable photoacid generators and without extensive effort to prepare. The inventors of these compounds were Crivello and Lam in the 1970s.[7−9] Generally, onium salts consist of two ions with clearly separated roles, when it comes to absorption, stability, or initiation efficiency properties. The cation represents the chromophore and determines all photochemistry-related properties. The anion affects the strength of the generated photoacid and therefore initiation efficiency and all polymer chemistry-related properties.[8]

For the FP of epoxy resins, the iodonium salt is first excited with UV photons and cleaved, followed by the abstraction of a hydrogen.[13] This is followed by the liberation of the superacid and the start of classical cationic polymerization (Figure 1a).[8,14] During the polymerization reaction, heat Δ is liberated (b). The liberated thermal energy is able to cleave the radical thermal initiator R−R. In addition, the front can be started with conventional heat sources at this point as well (c). Generated radicals decompose the onium salt, and HX is formed (d). Afterward, cationic polymerization can be initiated again to start over the self-sustaining cycle (back to step b). Previous work indicated versatile applications and high-efficiency curing with iodonium salts in radical-induced cationic FP (RICFP). The onium salt can be applied in pure epoxy resins[15] and in the production of composite materials or filled systems based on bisphenol-A-diglycidylether (BADGE) formulations.[16,17]

For cationic initiators, low nucleophilicity of their anion is desired for the initiation and propagation reaction. In an ideal system, the interaction of the propagating cation and the anion

Received: August 22, 2022
Accepted: September 23, 2022
Published: October 5, 2022

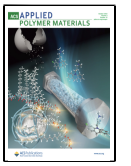

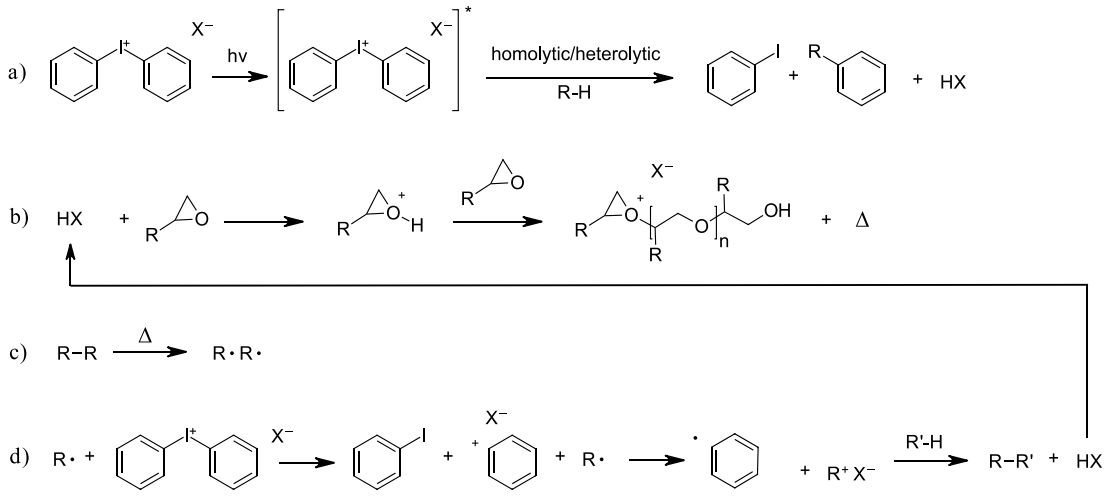

Figure 1. Reaction pathway of the photochemically and thermally initiated RICFP of an epoxy monomer.[10−12] (a) Photochemical decomposition of onium salts; (b) polymerization reaction; (c) radical thermal initiator cleavage; and (d) radical-induced decomposition of onium salts.

would be negligible. Therefore, a low nucleophilicity is directly related to a high rate of polymerization.[18] The reactivity of the used system correlates to the degree of separation of the cationic polymer chain and the anion and the stability of the anion itself.

The most accessible class of anions is represented by perfluorinated weakly coordinating anions (WCAs) like tetrafluoroborates, hexafluoroantimonates, hexafluorophosphates, and hexafluoroarsenates. Despite comprising a rather high nucleophilicity, these anions are broadly commercially available and usually easy to obtain as counterions of onium salts via metathesis reactions. Other stable WCAs with low nucleophilicity are represented by trifluoromethane-sulfonamides, teflate-based anions, or bridged alkoxy aluminates and borates.[19,20] Cyanide-bridged boranes are a large and well performing WCA, capable of polymerizing ethene.[21,22] Generally, the size of the anion is, among other things, directly responsible for lower nucleophilicity due to better charge distribution across the anion. The highly electron-withdrawing sulfonyl groups of the trifluoromethanesulfonamide are responsible for the ion's stability and its superacidic behavior.[23] This class of WCAs is usually applied as an ionic liquid, electrolyte, or catalyst.[24,25]

For applications in cationic photo- and FP, WCAs in combination with onium salts need to demonstrate low coordinative strength. Additionally, WCAs ideally show a certain tolerance toward moisture due to the usage of industrial monomers. Generally, such monomers measure a small water content.

In this paper, we explore different anions for state-of-the-art iodonium cations based on boron **B1**−**B5** (Figure 2). Up to now, they have usually been applied as ionic liquids especially in the field of electrolytes for lithium ion batteries.[24,25] These borate anions are then subject to investigations such as reactivity, stability, and versatility in general in epoxy-based resins. Small boron-based anions such as oxalatoborates as in **B3** and **B4** (Figure 2) promise rather low-molecular weight and very cheap starting materials. However, bridged boranes such as in **B1** are also of interest due to their promising outstandingly low nucleophilicity caused by the sheer size and therefore great charge distribution across the anion. First, the photoreactivity of the photoacid generators (PAGs) is the subject of investigation, followed by a thermal stability study of the formulations if thermally originated radicals are present. The collected data will give insights into each new PAG and its potential for FP. RICFP is conducted with all well performing synthesized iodonium salts either with photochemical or thermal initiation. Commercial and reference molecules consisting of three state-of-the-art PAGs are tested as well. **Com-Sb** and **Com-B1** represent two broadly used iodonium salts in industry. The iodonium aluminate **Ref-Al** demonstrates a state-of-the-art PAG developed by Klikovits et al. previously in this research group.[26] In combination with the radical thermal initiator 1,1,2,2-tetraphenyl-1,2-ethanediol (TPED), the frontal parameters, such as frontal velocity and frontal temperatures, are compared in an epoxy-based system.

2. EXPERIMENTAL PART

2.1. Materials and Methods. 4-(Octyloxyphenyl)phenyl iodonium hexafluoroantimonate (**Com-Sb**), 95%; CAS: 121239-75-6, ABCR; phenol, 99.5%, CAS: 108-95-2, TCI; 1-bromooctane, 99%, CAS: 111-83-1, Merck; potassium hydroxide, 99%, CAS: 1310-58-3, Fluka; iodobenzene diacetate, 98%, CAS: 3240-34-4 ABCR; 4-toluolsulfonic acid monohydrate, 98%, CAS: 6192-52-5, Carl Roth; acetic acid, 99%, CAS: 64-19-7, Fluka; oxalic acid anhydrous, 98%, CAS: 144-62-7, ABCR; lithium hydroxide, 99%, CAS: 1310-65-2, Carl Roth; boric acid, 99%, CAS: 10043-35-3, Merck; lithium fluoride, 99%, CAS: 7789-24-4, Carl Roth; sodium borohydride, 99%, CAS: 16940-66-2, Merck; dimethoxy ethane, 99%, CAS: 110-71-4, Merck; hexafluoroisopropanol, 99%, CAS: 920-66-1, Fluorochem; 1-bromo-2,3,4,5,6-pentafluorobenzene, 99%, CAS: 1074-91-5, TCI; *n*-butyllithium, 2.5 M in hexanes, CAS: 109-72-8, Merck; boron trichloride, 1 M in hexanes, CAS: 10294-34-5, Merck; potassium cyanide, 96%, CAS: 151-50-8, Merck; TPED, 95%, CAS: 464-72-2, TCI; 7-oxabicyclo[4.1.0]heptan-3-ylmethyl-7-oxabicyclo[4.1.0]heptane-3-carboxylate (ECC), 97%, CAS: 2386-87-0, BDL-Pharm; 1,6-hexanediol diglycidyl ether (HDDGE), POLYPOX R 18, CAS: 16096-31-4, DOW Chemical Company; and BADGE, Araldite MY 790-1, CAS: 1675-54-3, Huntsman. All chemicals and solvents were used as received if not mentioned otherwise in the synthesis section. NMR spectra were recorded on a Bruker Avance at 400 MHz for ^{1}H, 100 MHz for ^{13}C, 376 MHz for ^{19}F, and 128 MHz for ^{11}B. The signals were always referenced on the used NMR solvent with a deuterium grade of at least 99.5%.

2.2. Synthesis. The detailed synthesis of all alkali metal anions **K-B1**, **Li-B3**, **Li-B4**, and **Na-B5** and the final iodonium compounds **B1**, **B3**, **B4**, and **B5** is described in the Supporting Information. The synthetic pathway of the best performing system **B2** and its starting material **K-B2** is shown in the following section.

https://doi.org/10.1021/acsapm.2c01465
ACS Appl. Polym. Mater. 2022, 4, 7878−7890

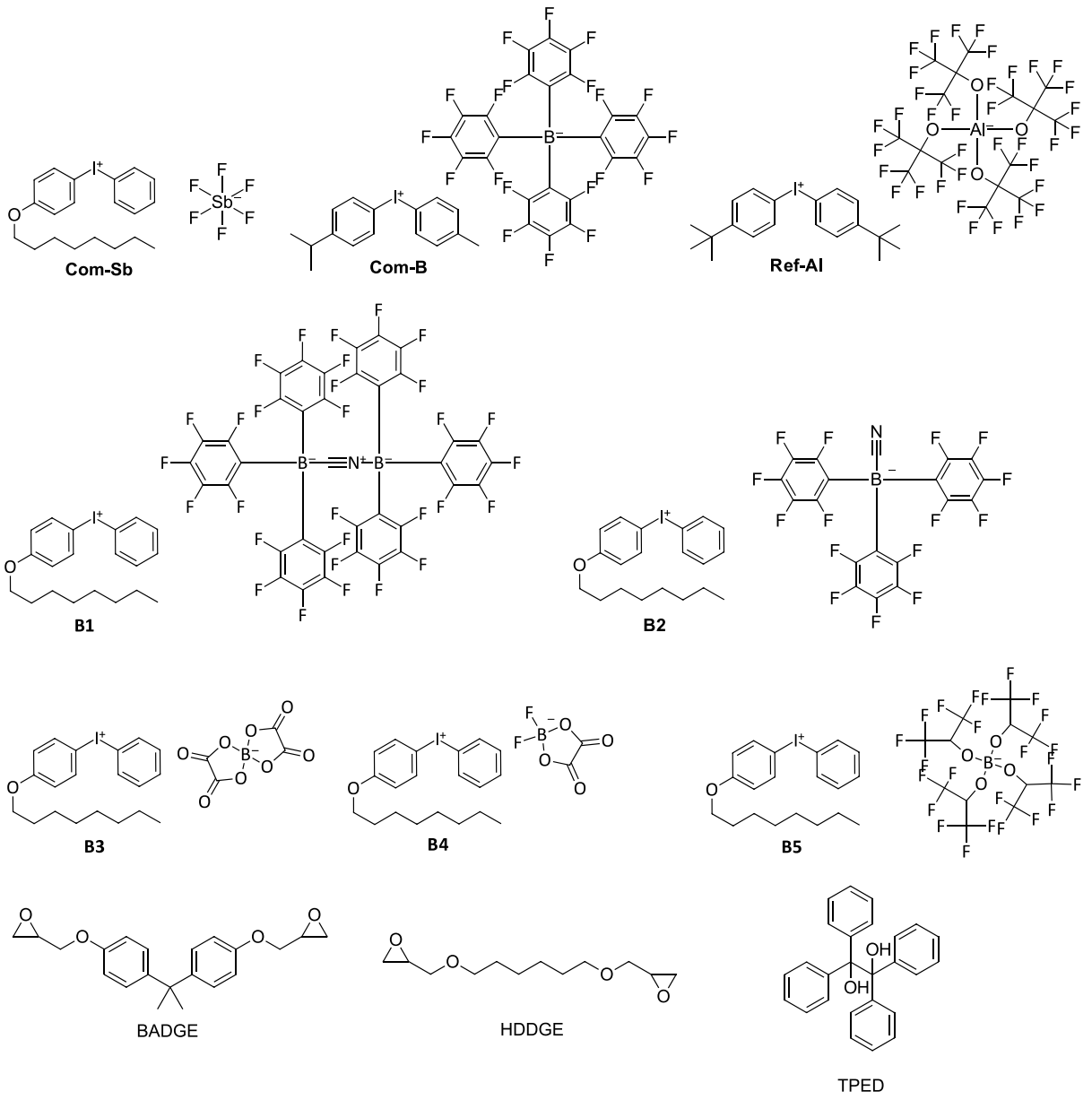

Figure 2. Iodonium salts **Com-Sb**, **Com-B1**, and **Ref-Al**[26] and **B1**, **B2**, **B3**, **B4**, and **B5**. Epoxy resins BADGE and HDDGE and the radical thermal initiator TPED. The epoxy monomer ECC is displayed in the Supporting Information.

*2.2.1. Potassium CN-[Tris(pentafluorophenyl)borane] (**K-B2**).* The product **K-B2** was synthesized similar to that of Zhou et al. (Figure 3c).[27] First, 1 equiv (307 mg, 0.6 mmol) of tris(2,3,4,5,6-pentafluorophenyl)borane was weighed into a 5 mL vial in a glovebox. Then, 3.5 mL of dry dichloromethane was added. The mixture was stirred at room temperature until the borane dissolved completely. In a separate vial, potassium cyanide was dissolved in deionized water, and 1 equiv (39 mg, 0.6 mmol, ~0.2 mL) of the solution was added to the borane solution. After 16 h of vigorous stirring at room temperature, 0.5 mL of deionized water was added, and the layers separated. The aqueous layer was washed twice with 4 mL of dichloromethane and twice with 4 mL of diethyl ether. The solvents were removed in vacuum on a rotary evaporator at room temperature. The product tends to foam during evaporation of the solvents. Finally, the synthesis route yielded 234 mg (68% of theory) of potassium CN-[tris(pentafluorophenyl)borane] as a white solid.

A faster workup procedure can be executed, if high yield is preferred over high purity. This route is sometimes advantageous if the salt is used in the next step as a precursor. After 16 h of stirring, the solvents are evaporated immediately without any water addition or extraction steps. Then, the viscous liquid is dissolved in 10 mL of dichloromethane, and the solvent evaporated quickly at the rotary evaporator at 30 °C. This process removes the minor amounts of water fast. Finally, K-BCN is obtained as a white solid in a yield of 99%.

Melting point: 57 °C (decomposition); ^{13}C NMR (100 MHz, DMSO): 148.9 (s, B$^-$−C≡N), 146.7 (s, 3× B$^-$−C), 139.1 (s, 6× B$^-$−C−CF), 137.4 (s, 6× B$^-$−C−CF−CF), 134.9 (s, 3× B$^-$−C−CF−CF−CF), 40.0 (sep, DMSO); ^{19}F NMR (376 MHz, DMSO): −134.7 (d, 6× B$^-$−C−CF), −162.2 (t, 3× B$^-$−C−CF−CF−CF), −165.9 (t, 6× B$^-$−C−CF−CF); ^{11}B NMR (128 MHz, DMSO): −4.20 (s, B).

*2.2.2. (4-Octyloxyphenyl)phenyl Iodonium CN-[Tris-(pentafluorophenyl)borane] (**B2**).* To synthesize **B2**, a metathesis reaction based on a patent by Castellanos et al. (Figure 3c)[28] was carried out. First, 0.95 equiv (255 mg, 0.44 mmol) of **K-B2** was dissolved in 3 mL of acetone and added dropwise to a solution of 1 equiv (267 mg, 0.46 mmol) of **I$^+$-Ts** in 5 mL of acetone with stirring at room temperature. A gel-like precipitate was formed. The suspension was stirred for 10 min and mixed with 4 mL of diethyl

https://doi.org/10.1021/acsapm.2c01465
ACS Appl. Polym. Mater. 2022, 4, 7878−7890

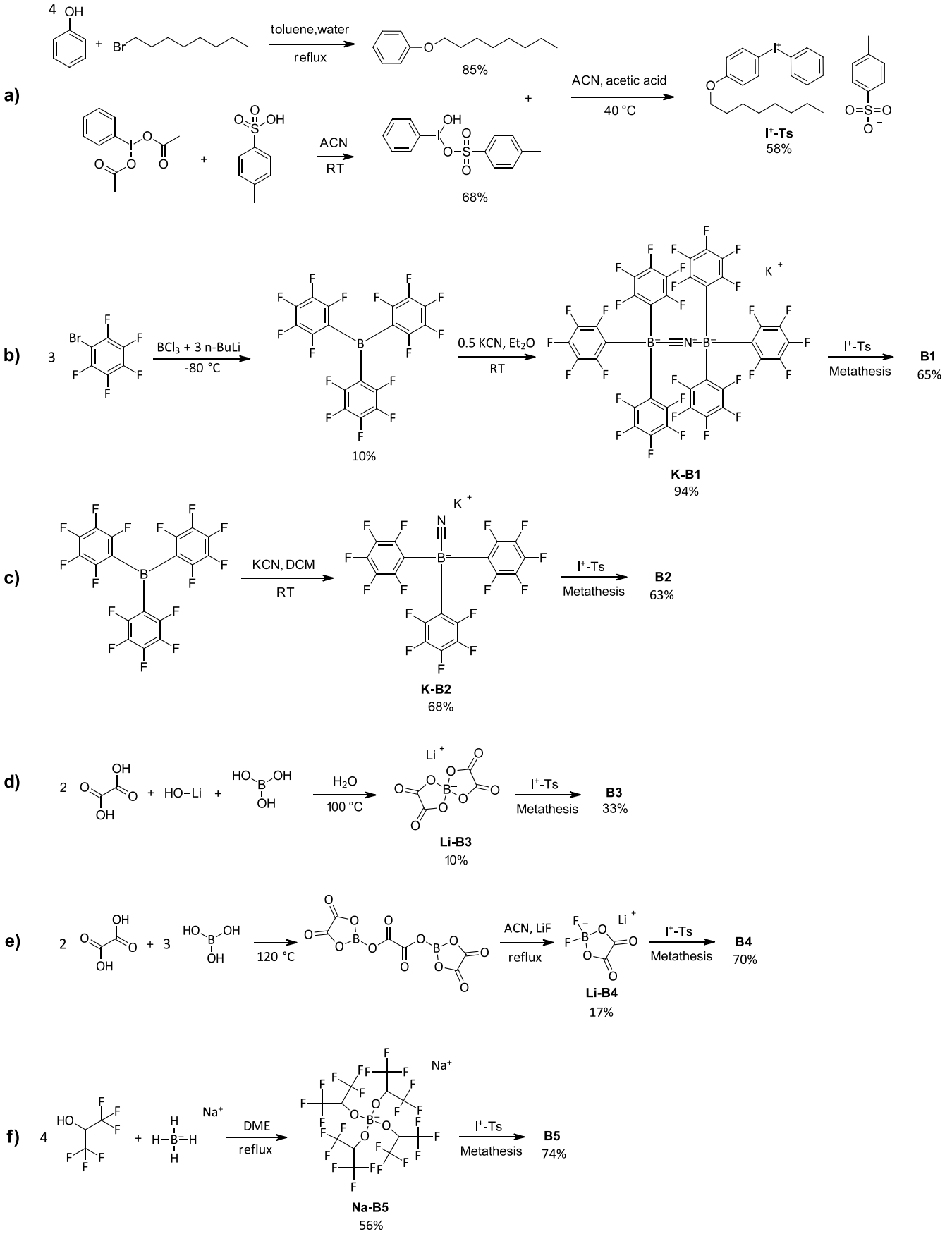

Figure 3. Synthesis pathways to the products (a) **I$^+$-Ts**; (b) **K-B1** and **B1**; (c) **K-B2** and **B2**; (d) **Li-B3** and **B3**; (e) **Li-B4** and **B4**; and (f) **Na-B5** and **B5**.

https://doi.org/10.1021/acsapm.2c01465
ACS Appl. Polym. Mater. 2022, 4, 7878−7890

ether, which corresponds to a ratio of the solvents of acetone/diethyl ether of 2:1. Additional diethyl ether was added until stirring of the gel-like precipitate was possible. The suspension was stirred for 10 min, centrifuged, and decanted and the solvent removed in vacuum. The yellow viscous residue was dissolved in 1 mL of acetone and mixed with 5 mL of diethyl ether, (solvent ratio 1:5). Additional diethyl ether was added until stirring of the gel-like precipitate was possible. After stirring for 10 min, the suspension was centrifuged, the solution decanted, and the solvents removed in vacuum. The potassium tosylate precipitate was discarded at this point in time. In order to remove **I$^+$-Ts** residues, flash column chromatography was carried out. The viscous yellow residue was dissolved in 2 mL of acetone and separated chromatographically with 30 mL of acetone over a glass frit filled with ∼2 g of silica gel. The solvent was removed in vacuum, and the residue was further dried in high vacuum overnight. A total of 274 mg (63% of theory) of (4-octyloxyphenyl)-phenyl iodonium CN-[tris(pentafluorophenyl)borane] was obtained as a sticky, colorless solid.

^{1}H NMR (400 MHz, DMSO): 8.20 (d, 2H, 2× I$^+$−C−C<u>H</u>−CH−CH), 8.15 (d, 2H, 2× I$^+$−C−C<u>H</u>−CH−C), 7.66 (t, 1H, C−CH−CH−C<u>H</u>), 7.53 (t, 2H, 2× I$^+$−C−CH−C<u>H</u>−CH), 7.06 (d, 2H, 2× I$^+$−C−CH−C<u>H</u>), 4.00 (t, 2H, O−C<u>H$_2$</u>), 2.50 (qui, DMSO), 1.69 (qui, 2H, O−CH$_2$−C<u>H$_2$</u>), 1.38 (qui, 2H, O−CH$_2$−CH$_2$−C<u>H$_2$</u>), 1.33−1.20 (m, 8H, O−CH$_2$−CH$_2$−CH$_2$−C<u>H$_2$</u>−C<u>H$_2$</u>−C<u>H$_2$</u>−C<u>H$_2$</u>), 0.85 (t, 3H, CH$_2$−C<u>H$_3$</u>); ^{13}C NMR (100 MHz, DMSO): 162.0 (s, O−<u>C</u>), 148.9 (s, B$^-$−<u>C</u>≡N), 146.7 (s, 3× B$^-$−<u>C</u>), 139.1 (s, 6× B$^-$−C−<u>C</u>F), 137.7 (s, 2× I$^+$−C−<u>C</u>H−CH−C), 137.4 (s, 6× B$^-$−C−CF−<u>C</u>F), 135.3 (s, 2× I$^+$−C−<u>C</u>H−CH−CH), 134.9 (s, 3× B$^-$−C−CF−CF−<u>C</u>F), 132.3 (s, C−CH−CH−<u>C</u>H), 132.1 (s, 2× I$^+$−C−CH−<u>C</u>H−CH), 118.3 (s, 2× I$^+$−C−CH−<u>C</u>H), 117.4 (s, I$^+$−<u>C</u>−CH−CH−CH), 105.5 (s, I$^+$−<u>C</u>−CH−CH−C), 68.5 (s, O−<u>C</u>H$_2$), 40.0 (sep, DMSO), 31.7 (s, O−CH$_2$−<u>C</u>H$_2$), 29.1 (s, O−CH$_2$−CH$_2$−<u>C</u>H$_2$), 29.1 (s, O−CH$_2$−CH$_2$−CH$_2$−<u>C</u>H$_2$), 28.8 (s, O−CH$_2$−CH$_2$−CH$_2$−CH$_2$−<u>C</u>H$_2$), 25.8 (s, O−CH$_2$−CH$_2$−CH$_2$−CH$_2$−CH$_2$−<u>C</u>H$_2$), 22.5 (s, O−CH$_2$−CH$_2$−CH$_2$−CH$_2$−CH$_2$−<u>C</u>H$_2$), 14.3 (s, CH$_2$−<u>C</u>H$_3$); ^{19}F NMR (376 MHz, DMSO): −134.7 (d, 6× B$^-$−C−C<u>F</u>), −162.2 (t, 3× B$^-$−C−CF−CF−C<u>F</u>), −165.9 (t, 6× B$^-$−C−CF−C<u>F</u>); ^{11}B NMR (128 MHz, DMSO): −4.20 (s, <u>B</u>) (Figure S2).

2.3. Preparation of Formulations Based on BADGE. The iodonium salts were used in 1.0 mol % referred to epoxy groups of BADGE or in 1.0 wt %, depending on the study. Additionally, the compound TPED was used in an equimolar amount compared to the iodonium salt. The mixtures were homogenized using a vortex device, followed by 30 min of ultrasonic bath treatment at around 40 °C and vortexed again to achieve a homogeneous formulation.

2.4. Photoreactivity by Photo-DSC. At first, the potential of the PAGs to efficiently initiate cationic polymerization was investigated. The prepared formulations were weighed in 12 ± 2 mg portions into small aluminum crucibles with a pipette. The crucible then was transported via an autosampler into the measuring chamber of a NETZSCH 204 F1 Phoenix photo-differential scanning calorimeter, which was flushed with nitrogen to maintain an inert atmosphere. There was also a second crucible, the empty reference. The polymerization was induced by UV light of an OMNICURE 3000 Series with a wavelength of 320 to 500 nm at an intensity of 136 mW cm^{-2} at the surface of the sample. The exotherm of the polymerization was recorded over time. The polymerization was carried out isothermally at 25 °C. The samples were exposed for 300 s. Three determinations were made per formulation. The temperature was set to 25, 50, 70, or 90 °C depending on the study.

The time to the highest exotherm is called t_{max} [s]. In the time-resolved differential scanning calorimetry (DSC) plot, this corresponds to that point in time at which the peak height h achieved its maximum. This value is then subtracted for 5 s as this time corresponds to the internal delay of the measuring device. To determine the time in which 95% of the conversion was achieved ($t_{95\%}$), the peak area ΔH_P (heat of polymerization) was integrated to cover 95% of the area between the integration limits. Peak height h [W g^{-1}] and the rate of polymerization R_P [mmol L^{-1} s^{-1}] correlate. Higher values resulted in higher reactivity of the measured system. The epoxy group conversions (EGCs) were determined via eq 1, and the R_P was calculated via eq 2. The theoretical heats of polymerization and the monomer densities were taken from Table 1.

Table 1. Theoretical Heats of Polymerization ($H_{P,0}$)[19] and Densities (ρ) of the Monomers

monomer	$H_{P,0}$[kJ mol^{-1}]	$H_{P,0}$[J g^{-1}]	ρ [g L^{-1}]
ECC	194	769	1170
BADGE	194	570	1160
HDDGE	194	842	1076

2.5. Thermal Stability by DSC. To test the thermal stability of the PAG-containing formulations, if thermally originated radicals are present, a simultaneous thermal analysis was performed. In addition, this study reveals the potential for the propagation step during RICFP. The formulations with 0.5 mol % onium salt and an equimolar amount of TPED, described in the previous "Preparation of Formulations" section, were used for all DSC measurements using a NETZSCH 449 F1 JUPITER equipped with an autosampler. The prepared formulations were weighed in 13 ± 3 mg portions into small aluminum crucibles, which were closed using a pierced lid. The crucible then was transported via the autosampler into the measuring chamber, which was flushed with nitrogen (40 mL min^{-1}) to maintain an inert atmosphere. The polymerization was induced by applying a temperature gradient. The temperature program started from 25 °C heating up to 350 °C at a rate of 10 K min^{-1}. Afterward, the samples were cooled down to 25 °C at a rate of 20 K min^{-1}. The exotherm behavior of the polymerization was recorded over time. Two determinations were made per formulation. The EGCs were determined via 1,[29] and R_P was calculated via 2.[30] The theoretical heats of polymerization and the monomer densities were taken from Table 1.

$$\text{EGC}\ [\%] = \frac{\Delta H_P}{\Delta H_{P,0}} \times 100 \tag{1}$$

ΔH_P—heat of polymerization of the sample [J g^{-1}] and $\Delta H_{P,0}$—theoretical heat of polymerization [J g^{-1}].

$$R_P \left[\frac{\text{mmol}}{\text{L·s}}\right] = \frac{h \times \rho}{H_{P,0} \times 1000} \tag{2}$$

h—corresponds to the heat produced per mass unit of the sample [W g^{-1}], ρ—density of the monomer [g L^{-1}], and $\Delta H_{P,0}$—theoretical heat of polymerization [J g^{-1}].

2.6. Radical-Induced Cationic FP. For the preparation of the formulations for the RICFP experiments, the iodonium salts were weighed into vials with 0.1, 0.25, and 0.5 mol % based on the epoxy groups of a monomer mixture of 80 mol % BADGE and 20 mol % HDDGE. Additionally, the compound TPED was used in an equimolar amount compared to the iodonium salt, and the mixtures were homogenized.

The respective formulations were then poured into a Teflon mold measuring 65 mm × 5 mm × 5 (length, width, depth) mm and then heated at one end with a focused infrared source (OPTRON IR-Spot 150 W; 10 mm focal point), which automatically switched off at 190 °C using an infrared (IR) sensor (OPTRON IN810 CF2).

In addition to the thermally initiated RICFP, an UV-light-initiated version was carried out as well. The formulations were poured in the same Teflon mold mentioned above, and an OMNICURE 3000 Series with a wavelength of 320 to 500 nm, at an intensity of 2.5 W cm^{-2} at the surface of the sample, was used as the irradiation source.

The FPs were then recorded with a thermal imaging camera (OPTRIS Xi 400). From the progression of the front through the sample, the frontal velocity v_F could then be calculated via 3.

$$v_F = \frac{l}{t} \tag{3}$$

https://doi.org/10.1021/acsapm.2c01465
ACS Appl. Polym. Mater. 2022, 4, 7878−7890

l—covered length of the front [cm] and t—time required to cover the length [min].

The covered length of the front was selected after the initiating point, from a defined length after the beginning of the shape to a defined length before the end of the shape.

The maximum front temperature T_F was determined by averaging the maximum front temperature at a defined length after the beginning of the mold and the maximum front temperature at a defined length before the end of the mold. Three measurements were performed per formulation.

The front starting time ($t_{F,s}$) represents the time interval from start of the UV irradiation until a stable FP is established.[6] However, this value is heavily influenced by the frontal velocity. Therefore, a correction factor, the frontal boundary time ($t_{F,b}$), is introduced. This value represents the time a front visibly passed a section 0.46 cm after the irradiation shield (distance d). This section is monitored using the IR camera, and as soon as the maximum temperature at this point is reached, $t_{F,b}$ can be determined. Knowing the frontal velocity and the distance d between the irradiation spot and the section, a defined length, after the irradiation shield, the frontal velocity-independent front starting time can be calculated4. For thermally initiated FP, no front starting time was calculated.

$$t_{F,s} = t_{F,b} - \frac{d}{v_F} \tag{4}$$

d—distance between the irradiation spot and a defined length (0.46 cm in this case) after the irradiation shield [cm].

2.7. Epoxy Group Conversion Determined via ATR-IR. The EGC of the composites cured by RICFP was determined using attenuated total reflection (ATR)-IR spectroscopy. The IR spectrum of the specimens was measured in the range of 4000 to 600 cm^{-1}. The band representing the epoxy group itself is located at a wavenumber of 914 cm^{-1}. As reference bands, the aromatic ring of the monomer BADGE (828 cm^{-1}) and the phenyl ether of BADGE (1183 cm^{-1}) were chosen. The EGC was calculated utilizing the ratios between the epoxy and the reference band of the starting formulations and the polymer samples 5. To allow for the dark curing effect, 2 days after the specimens were produced by RICFP, ATR-IR spectroscopy was carried out. Three measurements for each specimen were performed at three different locations across the sample.

$$\text{EPG [\%]} = \left(1 - \frac{\frac{A_{P,915}}{A_{P,ref}}}{\frac{A_{F,915}}{A_{F,ref}}}\right) \times 100 \tag{5}$$

$A_{P,915}$—integrated area of the epoxy IR band at 914 cm^{-1} of the final polymer [ ], $A_{P,ref}$—integrated area of the reference IR band at 828 or 1183 cm^{-1} of the final polymer [ ], $A_{F,915}$—integrated area of the epoxy IR band at 914 cm^{-1} of the initial formulation [ ], and $A_{F,ref}$—integrated area of the reference IR band at 828 or 1183 cm^{-1} of the initial formulation [ ].

2.8. RICFP of Thin Layers. In addition, in a mold with the dimensions of 95 mm × 5 mm (length, width), which rises continuously starting from 5 to 0.1 mm depth, the layer thickness at which the FP stops was measured.[31] Three measurements were performed per formulation.

2.9. Storage Stability Tests. For the storage stability tests, the iodonium salts were mixed with 80 mol % BADGE and 20 mol % HDDGE as mentioned in the "Radical-Induced Cationic FP" section. The iodonium salt was used in 0.5 mol % in combination with the same molar amount of TPED. The formulations were stored at a constant temperature of 50 °C under light exclusion. The storage stability was determined via rheology measurements using an Anton Paar MCR 300 rheometer. Around 80 μL of formulation was used each time. The gap size between the stamp and plate was set to 48 μm, and the shear rate was increased from 0 to 100 s^{-1} over 50 s. Afterward, five measurements of the viscosity were performed every 10 s to finally result in a measurement time of 100 s. The average value of these five measurement points was then calculated and displayed in the diagrams.

3. RESULTS AND DISCUSSION

3.1. Synthesis. An iodonium-based starting material for all the following metathesis reactions has to be synthesized first (Figure 3a). The best option is to synthesize an alkoxylated iodonium salt with a tosylate counter ion since this molecule is well known in the literature and easy to obtain.[28] Since the tosylate is not a WCA, much less nucleophilic anions are targeted, for example, antimonates, perfluorinated borates,[32] and aluminates.[26]

*3.1.1. Precursor (4-Octoxyphenyl)phenyl Iodonium Tosylate (**I^+-Ts**).* **I^+-Ts** represents the precursor to all subsequent iodonium salts in this study (Figure 3a). To synthesize octyl phenylether, a synthesis according to a patent by Castellanos et al. was carried out.[28] Hydroxy tosyloxy iodobenzene was prepared according to a synthesis based on the work of Cross et al.[33] To synthesize **I^+-Ts**, a procedure similar to that of the patent of Castellanos et al. was carried out to finally achieve an overall yield of 39%.[28]

*3.1.2. Anions (**K-B1, K-B2, Li-B3, Li-B4,** and **Na-B5**).* All synthesized anions are based on boron in combination with the alkali metal cation lithium, sodium, or potassium. Cyanide-bridged boranes represent very WCAs, which can be used as potential counterions for the iodonium salts.[22] In the first reaction step, bromopentafluorobenzene is converted to the perfluorinated trisborane with a yield of around 10% based on the work of Fischer and Schmidtmann.[34] Followed by the second step according to Zhou et al., the trisborane is treated with potassium cyanide to yield **K-B1** in high yields of 94% (Figure 3b).[27]

Very similar to the cyanide-bridged borane **B1**, the cyanide-ligated form **B2** was aimed for next. The anion was synthesized similar to the work of Zhou et al.[27] In this reaction route, a full equivalent of potassium cyanide was reacted with the perfluorinated trisborane resulting in 63% yield of **B2** (Figure 3c).

Oxalatoborates are relatively new WCAs and mainly used in lithium-ion battery research, as they are relatively cheap and perform well as electrolytes and as ionic liquids.[35,36] To synthesize lithium bis(oxalatoborate) **Li-B3**, a synthesis according to a patent by Lischka et al. was carried out by reacting lithium hydroxide with oxalic acid in water achieving a rather low yield of 10% (Figure 3d).[37]

Fluorinated oxalatoborates are used as stabilizing additives in electrolytes for lithium-ion batteries.[38] In the first reaction step, oxalic acid is reacted with boric acid according to a patent by Zhang et al. to form lithium difluoro(oxalato)borate. Finally, in the second step, lithium fluoride and acetonitrile are added to result in **Li-B4** in a yield of 17% (Figure 3e).[39]

Oxyborates are used in particular as high-performance anodes in lithium-ion batteries.[40,41] In the first reaction step, sodium borohydride is reacted with hexafluoroisopropanol according to a paper by Kaliner et al. to form sodium tetrakis((1,1,1,3,3,3-hexafluoropropan-2-yl)oxy)borate **Na-B5** in a yield of 56% (Figure 3f).[42]

*3.1.3. Iodonium Salts (**B1, B2, B3, B4,** and **B5**).* The previously synthesized anions are now subject to a salt metathesis reaction. During the process similar to a patent of Castellanos et al., the **I^+-Ts** precursor and the desired anion are dissolved in acetone.[28] By mixing the two solutions, the aimed iodonium salt including its new counterion forms in solution,

https://doi.org/10.1021/acsapm.2c01465
ACS Appl. Polym. Mater. 2022, 4, 7878−7890

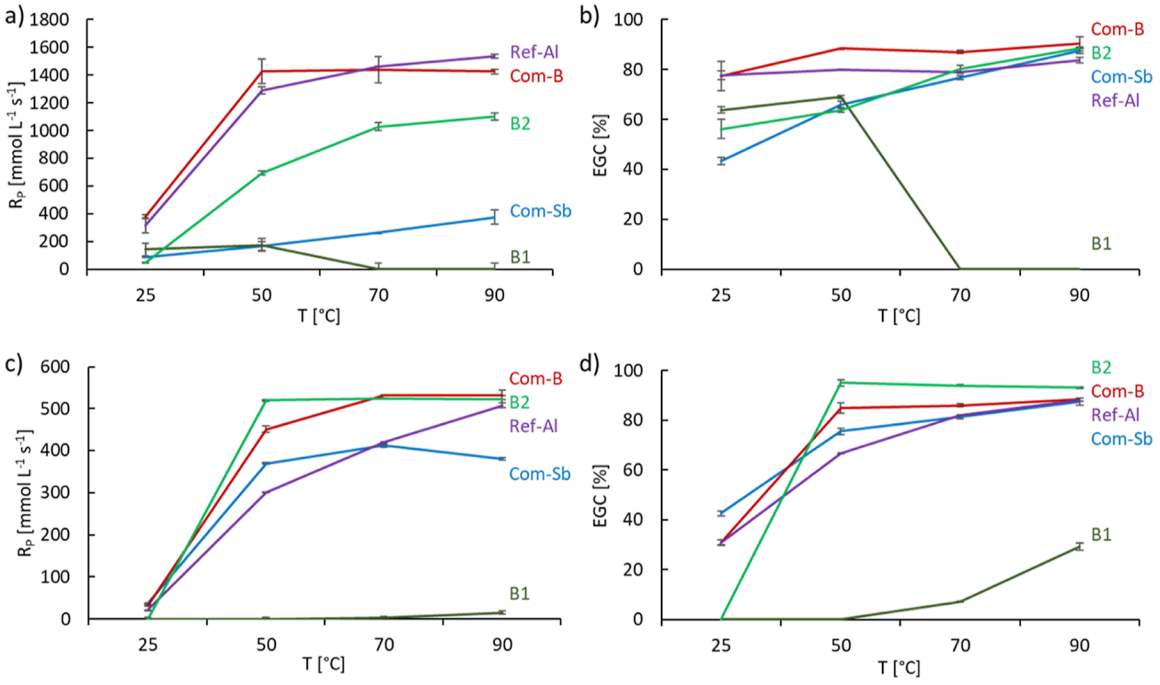

Figure 4. Photo-DSC: 1.0 mol % iodonium salt in BADGE at four different temperatures: (a) rate of polymerization (R_P) and (b) EGC. The data of **B2**, **B3**, and **B4** and additional parameters and data of samples based on the cycloaliphatic epoxy monomer ECC are depicted in Figure S4. Photo-DSC: 1.0 wt % iodonium salt in BADGE at four different temperatures: (c) rate of polymerization (R_P) and (d) EGC. The data of **B2**, **B3**, and **B4** and additional parameters and data of samples based on the cycloaliphatic epoxy monomer ECC are depicted in Figure S5.

while the byproduct alkali metal tosylate precipitates out of solution. The polarity of the solvent is decreased step by step with the addition of more diethylether. In the final purification step, remaining **I$^+$-Ts** impurities are removed by flash column chromatography over a small amount of silica gel. To synthesize the boron-based iodonium salts **B1**, **B3**, **B4**, **B5**, and **B2**, the reaction route described above was carried out with varying ratios of acetone to diethylether depending on the salt and yields between 33 and 74% (Figure 3).

3.2. Absorption Spectra Determined via UV−Vis Experiments. Considering onium salts in general, the cation is responsible for the photochemical properties such as absorption. As expected, the difference between the selected compounds is rather small due to high similarities of the iodonium cation (Figure S3). The reference compound **Com-Sb** and the self-synthesized PAGs **B1**, **B2**, **B3**, **B4**, and **B5** all contain the same alkoxylated cation and consequently show very similar absorption behavior starting at around 350 nm. In addition, the reference PAGs **Com-B1** and **Ref-Al** consist of a very similar alkylated iodonium cation and therefore show related spectra. All samples show, as expected for iodonium salts, an absorption maximum in the range of 250 nm.

3.3. Preparation of Formulations Based on BADGE. For measuring the thermal and photochemical properties of the synthesized PAGs, appropriate formulations have to be prepared. The iodonium salts show good solubility in a variety of commercially available epoxy monomers such as BADGE. Therefore, the iodonium salts are homogeneously dissolved in a concentration of 1.0 mol % in BADGE. Epoxy monomers like the bisphenol-A-based BADGE or the aliphatic HDDGE offer a non-polar environment which is well suited to dissolve the self-synthesized alkoxylated iodonium salts together with the commercial **Com-Sb** and alkylated commercial initiators **Com-B1** and **Ref-Al** (Figure 2). Additionally, an equimolar amount of TPED referred to the iodonium salt is added in some experiments (Figure 2). TPED is a C−C labile compound and used as a radical thermal initiator to subsequently decompose the iodonium salt upon heating.[6] A more industry-relevant formulation was prepared in addition, containing 1 wt % of the iodonium salt in BADGE (Figure S5).

3.4. Photoreactivity by Photo-DSC. To better understand the initiation efficiency and reactivity of the synthesized PAGs and the suitability of each PAG to start a photochemically initiated RICFP, photo-DSC was performed. If successful, formulations are highly likely to be suitable for photochemically initiated RICFP. Generally, the iodonium salts were mixed with BADGE as described in the Formulations section. Since the UV−vis experiments indicated very similar absorption spectra across the tested iodonium compounds, an irradiation source equipped with a 320−500 nm filter was used for all formulations. The photocleavage of the iodonium salt liberates the super acid and finally initiates cationic polymerization. The rate of polymerization R_P [mmol L^{-1} s^{-1}] correlates to the curing speed, and higher values resulted in higher reactivity of the measured system. The EGC is determined as the ratio of the experimentally measured heat of polymerization via DSC to the theoretical heat of polymerization of the epoxy system.

3.4.1. Photo-DSC Study Using Equimolar Conditions. The main objective of this study was to investigate the potentials of all iodonium salts as photoacid generators. To enable a fair comparison, the formulations consist of 1 mol % of iodonium-based PAG combined with the industrially relevant monomer BADGE. Additionally, the temperature dependence was investigated to draw a comparison between each of the initiators at 25, 50, 70, and 90 °C. Cationic polymerizations are known to be strongly temperature-dependent; therefore, it is advantageous to investigate a board temperature range.[43,44] In

https://doi.org/10.1021/acsapm.2c01465
ACS Appl. Polym. Mater. 2022, 4, 7878−7890

addition, a study at different temperatures is especially interesting due to the rise of technologies like hot lithography, which enable the application of highly viscous resins like BADGE. A benefit that comes along with the drop in viscosity is the increase in reactivity of the resin at elevated temperatures.

By comparing the data obtained by the photo-DSC measurements at four different temperatures, clear trends in reactivity can be seen (Figure 4a). Generally, the higher the temperature, the more reactive an initiator system behaves. **Com-B** and **Ref-Al** together with the new cyanide-ligated borane **B2** demonstrate high reactivity across a broad range of temperatures. **B2** reaches up to 1100 mmol L^{-1} s^{-1} at 90 °C in BADGE, which represents 71% of the reactivity of the best performing reference **Ref-Al**. Interestingly, the cyanide-bridged borane **B1** shows a rapid drop in reactivity starting at 70 °C due to thermolability. Polymerization of **B1** samples takes place as soon as the sample is inserted into the preheated DSC chamber; therefore, no more significant exothermicity can be recorded during the irradiation period. Upon comparing the EGC of all initiator systems, a clear trend can be obtained of most samples (Figure 4b). With the exception of that of **B1**, the EGC at 90 °C is between 90 and 84% across all systems with the best performance demonstrated by the commercial **Com-B** and **B2**. By directly comparing the structurally very similar commercial borate **Com-B** with the cyanide-ligated borane **B2**, a slight advantage for **Com-B** can be measured. This circumstance could be explained by the proposed higher coordinative strength of the **B2**'s anion compared to that of **Com-B**. The anion of **B2** consists of three pentafluoro phenyl rings and the cyanide ligand. The **Com-B**'s counterion shows four pentafluoro phenyl rings in its structure, making it probably a little less nucleophilic, hence less prone to undesired side reactions during polymerization.

In the cycloaliphatic monomer ECC, **B2** represents the best performing self-synthesized initiator, achieving 78% of the reactivity of the commercial **Com-Sb** (Figure S4c). The small PAGs **B3** and **B4** show similar performance compared to **B1** at around 20 mmol L^{-1} s^{-1}. According to the literature, all iodonium salts show the possibility for sensitization with an appropriate sensitizer such as anthracene.[45]

3.4.2. Photo-DSC Study Using the Same wt %. Previous photo-DSC experiments utilized formulations with 1 mol % of iodonium salt based on epoxy groups. Most industrial applications use for the sake of simplicity and more straightforward comparability regarding price formulations containing a set percentage of initiating species referred to weight. The formulations consist of 1 wt % of an iodonium-based photoacid generator in BADGE and were measured at 25, 50, 70, and 90 °C.

As expected, a clear trend toward increased rates of polymerization as temperature rises is present across all initiator systems (Figure 4c). A good example is presented by the commercial systems like the borate **Com-B1**, which increases its R_p from 32 mmol L^{-1} s^{-1} at 25 °C up to 533 mmol L^{-1} s^{-1} at 90 °C. If comparing the performance of the cyanide-bridged borane **B1** to the study with 1 mol % in BADGE, the clear disadvantage of such high-molecular weight initiators in this 1 wt % study can be seen compared to iodonium salts with lower-weight counter ions. Most of the self-synthesized iodonium salts do not show great reactivity across any temperature investigated in the study with the exception of **B2**. The cyanide-ligated **B2** provides excellent reactivity, even outperforming all commercial systems at 50 °C with an R_p of 520 mmol L^{-1} s^{-1}. This polymerization rate is 41, 15%, and an astonishing 73% higher compared to that of **Com-Sb**, **Com-B1**, and **Ref-Al**, respectively. Its striking that **B2** as an initiator system reaches increased EGC compared to the commercial systems at 93% up to 95% (Figure 4d). Interestingly, **B2** samples at 25 °C turn out to be solid after the irradiation procedure. However, no rate of polymerization can be calculated due to no measurable exotherm behavior during the DSC experiments. This unusual behavior can be explained by the reproducible crystallization of BADGE in **B2** formulations in the aluminum crucibles at 25 °C. Therefore, the polymerization signal is overlapped and compensated for by an endothermic melting of the resin using the UV source. By comparing t_{max} and $t_{95\%}$ values, an obvious trend toward lower values can be seen as temperature increases (Figure S5b). At room temperature, the commercial system **Com-B1** delivers the fastest polymerization parameters. If the temperature is increased, a rather similar pattern regarding t_{max} and $t_{95\%}$ can be obtained across all commercial iodonium salts and the self-synthesized **B2**.

By comparing the 1 mol % with the 1 wt % data (Figure 4a,c), it seems counterintuitive to have an inverse trend for the cyanide-bridged borane **B1**. The amount of **B1** in the formulations varies heavily by a factor of 8.6 if using weight percentages compared to molar ratios. The thermolabile behavior of the **B1**'s anion leads to pre-polymerization in the photo-DSC measurement chamber starting at 70 °C with high amounts of the initiator present (mol %). Therefore, the polymerization reaction is already finished in the isothermal phase, leaving no significant number of reactive epoxy groups for the irradiation phase, where the exotherm peak usually occurs. For the 1 wt % study, around one-ninth of **B1** is present in the formulation. This leads to insignificant reactivities at 25 and 50 °C. Since the polymerization rate of the lower-amount **B1** formulations (wt %) is lower, the pre-polymerization at 70 and 90 °C is much slower compared to that of the molar ratio study. Therefore, a significant number of epoxy groups are still available for polymerization as soon as the isothermal phase is over and the irradiation phase starts, leading to a lower measured reactivity at higher temperatures for **B1** in the mol % study.

3.5. Thermal Stability by DSC. DSC of all formulations containing an equimolar amount of different cationic initiators and the thermal initiator TPED was performed. This method shows the potential propagation behavior during FP. If a high reactivity of the initiator and TPED pair can be achieved, the probability of a working RICFP is very high. The iodonium salts were mixed with the C−C labile compound TPED in BADGE as described in the Formulations section. By exposure to the fixed temperature gradient, TPED cleaves, and its radicals decompose the onium salt. Therefore, a radical-induced cationic polymerization takes place (RICP). The temperature at which the polymerization started is called T_{onset} [°C]. The rate of polymerization R_p [mmol L^{-1} s^{-1}] correlates to the curing speed, and higher values resulted in higher reactivity of the measured system. The EGC is determined via the ratio of the experimentally measured heat of polymerization via DSC to the theoretical heat of polymerization of the epoxy system.

As expected, the onset temperatures of the polymerization are in a similar range for most iodonium salts below 135 °C with the lowest temperature obtained for systems containing

https://doi.org/10.1021/acsapm.2c01465
ACS Appl. Polym. Mater. 2022, 4, 7878−7890

Com-B1 at 105 °C (Figure 5a). The commercial iodonium salts show the highest polymerization rates (Figure 5b).

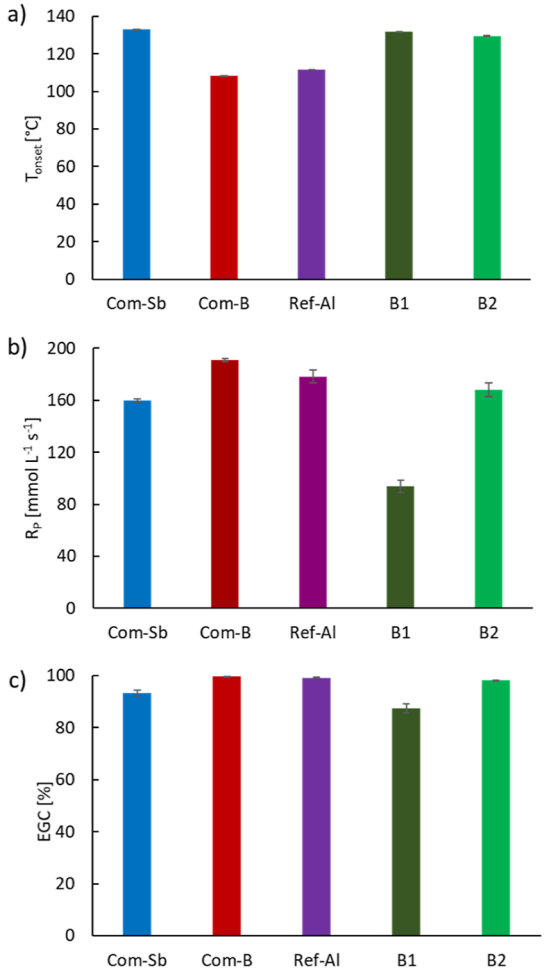

Figure 5. STA: 1.0 mol % iodonium salt and TPED in BADGE: (a) polymerization onset temperature (T_{onset}); (b) rate of polymerization (R_P); and (c) EGC. The data of **B3**, **B4**, and **B5** and additional parameters and data of samples based on the cycloaliphatic epoxy monomer ECC are depicted in Figure S6.

Surprisingly, the new initiator **B2** performs in a similar range. Additionally, **B2** achieves an outstanding EGC of 98% (Figure 5c). **B1** shows good conversions of above 88%. The remaining initiators **B4** and **B5** show the highest onset temperature across all self-synthesized initiators at 143 °C (Figure S6a). The iodonium-based salts **B2** and **B1** together with the commercial salts **Com-Sb**, **Com-B1**, and **Ref-Al** show very good results and show great potential for a successfully propagating FP.

In the cycloaliphatic monomer ECC, **B5** even shows about 50% of the rate of polymerization compared to the commercial **Com-B1** (Figure S6e).

3.6. Radical-Induced Cationic FP. A working RICFP requires either photochemical or thermal initiation depending on the properties of the formulations. By combining the results from the Photo-DSC and DSC section, excellent potential for both initiation pathways by the cyanide-ligated borane **B2** and good potential by the cyanide-bridged borane **B1** can be expected. First, the onium salts and TPED were dissolved in various concentrations in a monomer mixture of 80 mol % BADGE and 20 mol % HDDGE. Previous research suggests BADGE/HDDGE mixtures and suitable epoxy resins for RICFP.[46] The role of HDDGE in the formulations is to act as a reactive diluent to decrease viscosity and enhance reactivity of the resin. All iodonium salts (Figure 2) were used in 0.1, 0.25, and 0.5 mol % based on epoxy groups, and an equimolar amount of TPED was added. The formulations were then poured into a Teflon mold and photochemically initiated (Figure S7a). The FP reaction was then observed using a thermal imaging camera. For the UV-initiated RICFP, the front starting time $t_{F,s}$ [s] was calculated to evaluate the plainness of the formulations to start an FP. For some industrial applications, it is easier to start the RICFP directly by heat input. Therefore, the formulations in the Teflon molds were thermally irradiated with a focused IR source (Figure S7b). This source heated the formulation at the edge of the mold, and due to the temperature sensor, it was switched off automatically as soon as 190 °C was reached. This temperature was defined as sufficient temperature to initiate the FP since the onset temperatures of all PAGs as determined in the DSC section are well below this threshold.

Important parameters for the propagation of both photochemically and thermally initiated FP are the frontal velocity v_F [cm min^{-1}], correlating with the speed with which the local reactive zone spreads, and the maximum front temperature T_F [°C].

The front starting times for **Com-B1**, **Ref-Al**, and **B2** are quite similar in the range of 10.6 s for **Com-B1** up to 13.5 s for **Ref-Al** (Figure 6a). The self-synthesized **B2** performs better compared to the aluminate and nearly on par with the commercial borate. Interestingly, the commercial antimonate **Com-Sb** and the self-synthesized **B1** do not show the potential for photochemically initiated FP. Both **Com-Sb** and **B1** samples are not able to reach sufficient exothermicity to cleave enough TPED during polymerization to sustain an FP. An increase in the concentration can lead to stable FP for such initiation systems.[6]

To determine parameters such as frontal velocity and temperature, a thermally initiated FP was performed as well. For the formulations that were able to be initiated photochemically, these parameters stay equal if initiated thermally (Figure S9). This circumstance originates due to the frontal parameters of formulations being an inherent property of the system. As soon as a stable front is established, it propagates unchanged no matter if initiated thermally or photochemically. The focused IR source has a rated power output of 150 W at a focal point a few millimeters in diameter, whereas the UV source delivers 2.5 W cm^{-1} to the surface of the sample. For UV applications, the seemingly low power output is actually very high and usually in the mW range as stated in the Photo-DSC section.

The cyanide-ligated borane **B2** reaches similar performance as the commercial iodonium salts **Com-B1** and **Ref-Al** with a maximum velocity v_F of around 11.5 cm min^{-1} at a concentration of 0.5 mol % (Figure 6b). The next best compound is the cyanide-bridged borane **B1**, performing even better than the most commonly used commercial initiator **Com-Sb**. Even at a lower concentration of 0.1 and 0.25 mol %, the FP obtained by **B2** reaches similar velocities compared to that obtained by the state-of-the-art borate **Com-B1**.

Considering the maximum front temperature T_F of all tested iodonium salts, a range can be obtained starting from 215 to 266 °C regardless of the concentration used (Figure 6c). The highest temperatures are measured within the **Com-B1**

https://doi.org/10.1021/acsapm.2c01465
ACS Appl. Polym. Mater. 2022, 4, 7878−7890

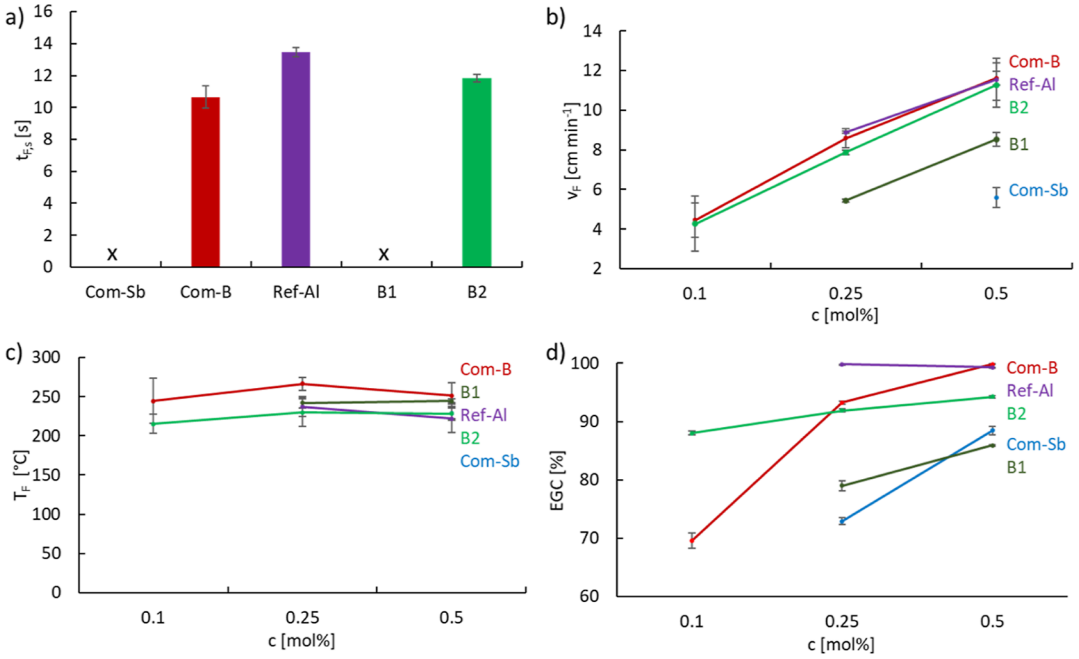

Figure 6. RICFP: 0.5 mol % iodonium salt with an equimolar amount of TPED in 80 mol % BADGE and 20 mol % HDDGE: (a) front starting time ($t_{F,s}$). Non-working UV-initiated FPs are marked with *x*. RICFP: 0.1, 0.25, and 0.5 mol % iodonium salt with an equimolar amount of TPED in 80 mol % BADGE and 20 mol % HDDGE: (b) frontal velocity (v_F); (c) frontal temperature (T_F); and (d) EGC of the specimens after RICFP.

samples at a maximum of 266 °C at 0.25 mol % initiator. However, **B2** samples show slightly lower values compared to commercial products of 215 °C at 0.1 mol % and 230 °C at 0.25 and 0.5 mol %. Lower front temperatures prevent high thermal stress to the material and therefore discoloration.

A visual inspection of the specimens after FP is performed (Figure 7). At a concentration of 0.1 mol % with the initiator

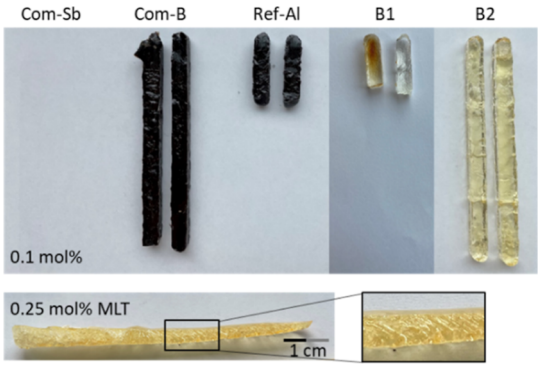

Figure 7. Specimens produced via thermally initiated RICFP of BADGE/HDDGE with an iodonium salt/TPED concentration of 0.1 mol %, based on epoxy groups. **Ref-Al** and **B1** specimens are shorter due to non-stable FP, and **Com-Sb** is missing completely due to insufficient reactivity; the horizontal specimen in addition to the magnified section exemplarily represents the MLT process for a **B2** sample at 0.25 mol %; pictures of specimens at 0.25 and 0.5 mol % are depicted in Figure S8.

B2, a bubble-free, clear specimen can be obtained. However, the specimen shows slight stickiness at the contact area between the Teflon mold, while **Com-B1** and **Ref-Al** samples show slightly better curing behavior at such low loadings. Already non-sticky samples with astonishing EGC can be obtained with a concentration of 0.25 mol % of **B2** to result in yellow specimens, which are non-transparent. Missing sample specimens like the **Com-Sb** at 0.1 mol % indicate a non-successful FP at that concentration. If the propagating reactive zone stops at any point during testing caused by insufficient reactivity, shorter specimens are presented. Examples of such a prematurely interrupted FP are **Ref-Al** and **B1** at 0.1 mol % loading. In addition, **B2**-based formulations produce slightly yellow-colored samples unlike the other commercial compounds, which produce black specimens.

3.7. Epoxy Group Conversion Determined via ATR-IR.

After successful FP experiments, the EGC of the specimens cured by RICFP was determined using ATR-IR spectroscopy. The EGC was calculated by the difference of the epoxy band integral before and after polymerization took place. Due to ring opening of the epoxide moiety, an aliphatic ether is formed. The decrease in area of the epoxy band (914 cm^{-1}) correlates with the EGC value.

A clear trend in EGC can be obtained for all samples after RICFP. As expected, higher initiator loadings lead to an increase in EGC (Figure 6d). The highest overall EGC is achieved by iodonium aluminate **Ref-Al** and the borate **Com-B** at 99% for all tested concentrations. The best performing self-synthesized iodonium salt is **B2** with an EGC of up to 94% and therefore close to that of the reference and commercial system. The frequently used initiator **Com-Sb** can achieve an EGC of 88% if a concentration of 0.5 mol % of the initiator is used. The new initiator **B1** performs at the same level.

3.8. RICFP of Thin Layers.

Epoxy resins are most commonly applied in thin films as decorative and protective coatings. Therefore, it is highly interesting to investigate the minimum layer thickness (MLT) an FP can sustain to ideally open a broad field of applications. The MLT of a sample was determined in the following experiments. The thinner the layer, in which a stable FP is possible, the more reactive is a system. An ascending Teflon mold (Figure S7c) was used to measure the MLT at which the FP stops.[31] The well-performing formulations with low initiator loadings (0.1 and

https://doi.org/10.1021/acsapm.2c01465
ACS Appl. Polym. Mater. 2022, 4, 7878−7890

0.25 mol %) were tested containing the iodonium salts **Com-B1**, **Ref-Al**, **B2**, and **B1** in a mixture of BADGE and HDDGE. Three samples were analyzed per formulation.

It can be clearly seen that very similar MLTs are achieved by the self-synthesized **B2** compared to those achieved by the state-of-the-art salts **Com-B1** and **Ref-Al** at around 4.1 mm (Figure 8). When the concentrations of the iodonium salt and

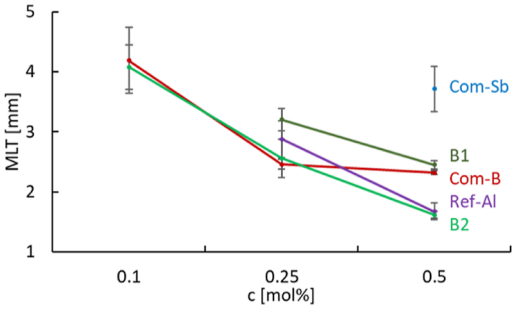

Figure 8. RICFP: 0.1, 0.25, and 0.5 mol % iodonium salt with an equimolar amount of TPED in 80 mol % BADGE and 20 mol % HDDGE: MLT of the specimens.

radical thermal generator TPED are increased to 0.25 and 0.5 mol %, respectively, the MLTs shrink as expected. Within small deviation, all initiators deliver from 3.2 mm down to 2.5 mm of MLT. Best performers at 0.25 mol % are the commercial borate **Com-B1** and the new cyanide-ligated borane **B2** with 2.5 mm MLT (Figure 7). By increasing the concentration to 0.5 mol %, the best performance is obtained with samples containing **B2** and **Ref-Al** at 1.7 mm MLT. Interestingly, **Com-B1** stagnates regarding MLT performance from 0.25 to 0.5 mol % initiator concentration. This counterintuitive observation can be explained by significant bubble formation at 0.5 mol % with **Com-B1** leading to heat dissipation and an overall higher MLT.

The data obtained in the RICFP experiments demonstrates the performance of the single ligated borane **B2** due to the on-par reactivity in frontal formulations compared to that of state-of-the-art salts, achieving only yellow-colored samples with the same frontal velocity, lower frontal temperature, and similar MLT values compared to the best performing commercial counterparts forming black-colored samples.

3.9. Storage Stability Tests. One major advantage of the RICFP compared to other epoxy-curing techniques is the enhanced pot life of the formulations. There is no need for a two-component system since all the necessary compounds for RICFP are mixed in advance and can usually be stored over several days without decreasing the performance significantly.[6] Therefore, a storage stability study was carried out at a constant storage temperature of 50 °C for all iodonium salts under light protection. The focused-on metric in terms of stability of a formulation was the viscosity, which was measured with a rheometer.

Initial viscosity for all formulations is around 1 Pa s. Unfortunately, poor shelf life of the commercial boron-based **Com-B1** and the self-synthesized **B1** at 50 °C can be seen (Figure 9). After 3 days, the viscosity starts to increase rapidly to finally result in a gel-like state on day 6. The formulations based on **Com-Sb**, **Ref-Al**, and **B1** show much better stability. The best performing salt is the aluminate **Ref-Al** with nearly no increase after 30 days. The commercial **Com-Sb** shows a significant increase starting after 2 weeks and reaching 7.5 Pa s

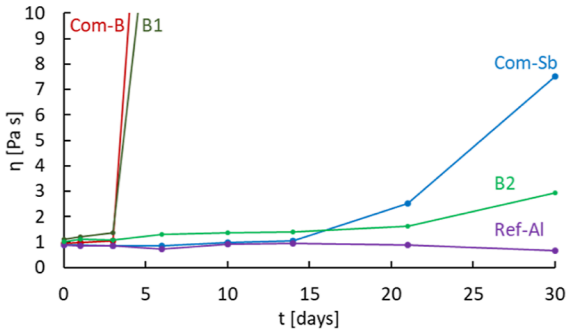

Figure 9. Time-dependent viscosity of 0.5 mol % iodonium salt/TPED at a storage temperature of 50 °C under light protection in BADGE/HDDGE. Data of samples based on BADGE and the cycloaliphatic epoxy monomer ECC are depicted in Figure S10.

after 1 month. Interestingly, the bridged borane **B2** shows much better performance compared to the commercial boron-based salts **Com-B1** or the structurally very similar **B1** with 2.9 Pa s after 30 days.

4. CONCLUSIONS

The main focus of this study was the synthesis of new anions for iodonium salts, suitable for cationic polymerization, especially RICFP. Due to its very fast and energy-efficient curing of monomers, this technique remains highly interesting. These newly synthesized PAGs **B1**−**B5** were mixed with commercially available epoxy monomers BADGE and BADGE/HDDGE to determine their reactivity via various DSC experiments. Their performance was compared with that of commercial state-of-the-art iodonium products **Com-Sb**, **Com-B1**, and **Ref-Al**.

Unfortunately, the iodonium salts with the small borate anions **B3** and **B4** do not demonstrate the potential to be an applicable cationic initiator. However, the new boron-based cationic initiator **B2** shows on-par or even better performance in terms of reactivity compared to its commercial counterpart **Com-B1**. Upon evaluating the industry-relevant 1.0 wt % PAG formulations at four temperatures in photo-DSC, the stunning performance of **B2** in BADGE across a broad range of temperatures can be seen (Figure 4c,d), even outperforming that of any commercial and reference system in terms of reactivity and EGC at 50 °C. The molecular weight of the cyanide-ligated anion in **B2** is 21 and 44% lower compared to that of the state-of-the-art PAGs **Com-B1** and **Ref-Al**, respectively. This advantage of lower molecular mass and easy synthetic access in combination with its high reactivity in all tested systems leaves **B2** as a novel, highly interesting initiator for cationic polymerization and RICFP. Stable and reproducible fronts could be obtained for all investigated concentrations from 0.5 mol % down to 0.1 mol % for **B2**. Even at a very low concentration of 0.1 mol % based on the epoxy groups, **B2** remains highly reactive and achieves together with **Com-B1** the highest fontal velocities. After curing, the **B2** samples appear transparent and slightly yellowish at a concentration of 0.1 mol %, unlike the black, non-transparent specimens produced by **Com-B1** and **Ref-Al**. This observation can be explained with low frontal temperatures of **B2** compared to those of the commercial and reference systems. Together with **Ref-Al**,[26] the new **B2** marks the second highly reactive cationic initiator developed in the research group.

https://doi.org/10.1021/acsapm.2c01465
ACS Appl. Polym. Mater. 2022, 4, 7878−7890

■ ASSOCIATED CONTENT

Supporting Information

The Supporting Information is available free of charge at https://pubs.acs.org/doi/10.1021/acsapm.2c01465.

NMR codes of all compounds including various spectra of **B1** and **B2**, UV−vis spectra, additional temperature-dependent photo-DSC results in BADGE and ECC, additional DSC results in BADGE and ECC, experimental RICFP setups, pictures of specimens after RICFP, thermally versus photochemically initiated RICFP results, and additional storage stability data in BADGE and ECC (PDF)

■ AUTHOR INFORMATION

Corresponding Author

Patrick Knaack − *Institute of Applied Synthetic Chemistry, TU Wien, 1060 Vienna, Austria;* orcid.org/0000-0001-9984-9087; Email: patrick.knaack@tuwien.ac.at

Authors

Roland Taschner − *Institute of Applied Synthetic Chemistry, TU Wien, 1060 Vienna, Austria*

Robert Liska − *Institute of Applied Synthetic Chemistry, TU Wien, 1060 Vienna, Austria*

Complete contact information is available at: https://pubs.acs.org/10.1021/acsapm.2c01465

Notes

The authors declare no competing financial interest.

■ ACKNOWLEDGMENTS

The authors acknowledge TU Wien Bibliothek for financial support through its Open Access Funding Program.

■ REFERENCES

(1) Chechilo, N. M.; Enikolop, N. S. Structure of Polymerization Wave Front and on Mechanism of Polymerization Reaction Spreading. *Dokl. Akad. Nauk SSSR* **1974**, *214*, 1131−1133.

(2) Khanukaev, B. B.; Kozhushn, M. A.; Enikolop, N. S. Theory of Polymerization Front Propagation. *Dokl. Akad. Nauk SSSR* **1974**, *214*, 625−628.

(3) Aleksanyan, G. G.; Arutyunyan, K. A.; Bodneva, V. L.; Davtyan, S. P.; Prut, E. V.; Rozenberg, B. A.; Shkadinskii, K. G.; Enikolopyan, N. S. Some Regularities of Propagation of Radical Polymerization Front of Vinyl Monomers. *Vysokomol. Soedin. A+* **1975**, *17*, 913−918.

(4) Pojman, J. A. Traveling Fronts of Methacrylic-Acid Polymerization. *J. Am. Chem. Soc.* **1991**, *113*, 6284−6286.

(5) Bynum, S.; Tullier, M.; Morejon-Garcia, C.; Guidry, J.; Runnoe, E.; Pojman, J. A. The effect of acrylate functionality on frontal polymerization velocity and temperature. *J. Polym. Sci., Part A: Polym. Chem.* **2019**, *57*, 982−988.

(6) Bomze, D.; Knaack, P.; Liska, R. Successful radical induced cationic frontal polymerization of epoxy-based monomers by C-C labile compounds. *Polym. Chem.* **2015**, *6*, 8161−8167.

(7) Crivello, J. V.; Lam, J. H. W. Diaryliodonium Salts—New Class of Photo-Initiators for Cationic Polymerization. *Macromolecules* **1977**, *10*, 1307−1315.

(8) Crivello, J. V. The discovery and development of onium salt cationic photoinitiators. *J. Polym. Sci., Part A: Polym. Chem.* **1999**, *37*, 4241−4254.

(9) Crivello, J. V.; Lam, J. H. W. Photoinitiated Cationic Polymerization with Triarylsulfonium Salts. *J. Polym. Sci., Polym. Chem. Ed.* **1979**, *17*, 977−999.

(10) Klikovits, N.; Liska, R.; D'Anna, A.; Sangermano, M. Successful UV-Induced RICFP of Epoxy-Composites. *Macromol. Chem. Phys.* **2017**, *218*, 1700313.

(11) Sangermano, M.; Antonazzo, I.; Sisca, L.; Carello, M. Photoinduced cationic frontal polymerization of epoxy-carbon fibre composites. *Polym. Int.* **2019**, *68*, 1662−1665.

(12) Abdul-Rasoul, F. A. M.; Ledwith, A.; Yagci, Y. Thermal and Photo-Chemical Cationic Polymerizations Induced by Agpf6 in Presence of Free-Radical Initiators. *Polym. Bull.* **1978**, *1*, 1−6.

(13) Dadashi-Silab, S.; Doran, S.; Yagci, Y. Photoinduced Electron Transfer Reactions for Macromolecular Syntheses. *Chem. Rev.* **2016**, *116*, 10212−10275.

(14) Bulut, U.; Crivello, J. V. Investigation of the reactivity of epoxide monomers in photoinitiated cationic polymerization. *Macromolecules* **2005**, *38*, 3584−3595.

(15) Bomze, D.Radical induced Cationic Frontal Polymerization as a new and versatile Curing Technique for Epoxy Resins. Doctoral Dissertation, Technische Universität Wien, 2016; p 105 ff.

(16) Bomze, D.; Knaack, P.; Koch, T.; Jin, H. F.; Liska, R. Radical Induced Cationic Frontal Polymerization as a Versatile Tool for Epoxy Curing and Composite Production. *J. Polym. Sci., Part A: Polym. Chem.* **2016**, *54*, 3751−3759.

(17) Tran, A. D.; Koch, T.; Knaack, P.; Liska, R. Radical induced cationic frontal polymerization for preparation of epoxy composites. *Composites, Part A* **2020**, *132*, 105855.

(18) Green, W. A.Cationic chemistry. *Industrial Photoinitiators: A Technical Guide*; Taylor & Francis: Boca Raton, 2010; Chapter 7, p 149.

(19) Riddlestone, I. M.; Kraft, A.; Schaefer, J.; Krossing, I. Taming the Cationic Beast: Novel Developments in the Synthesis and Application of Weakly Coordinating Anions. *Angew. Chem., Int. Ed.* **2018**, *57*, 13982−14024.

(20) Krossing, I.; Raabe, I. Noncoordinating anions—Fact or fiction? A survey of likely candidates. *Angew. Chem., Int. Ed.* **2004**, *43*, 2066−2090.

(21) Lancaster, S. J.; Walker, D. A.; Thornton-Pett, M.; Bochmann, M. New weakly coordinating counter anions for high activity polymerisation catalysts: [(C6F5)(3)B-CN-B(C6F5)(3)](-) and [Ni{CNB(C6F5)(3)}(4)](2-). *Chem. Commun.* **1999**, 1533−1534.

(22) Zhou, J. M.; Lancaster, S. J.; Walker, D. A.; Beck, S.; Thornton-Pett, M.; Bochmann, M. Synthesis, structures, and reactivity of weakly coordinating anions with delocalized berate structure: The assessment of anion effects in metallocene polymerization catalysts. *J. Am. Chem. Soc.* **2001**, *123*, 223−237.

(23) Nie, J.; Kobayashi, H.; Sonoda, T. Copper(II)bis-((trifluoromethyl)sulfonyl)amide. A novel Lewis acid catalyst in Diels-Alder reactions of cyclopentadiene with methyl vinyl ketone. *Catal. Today* **1997**, *36*, 81−84.

(24) Aravindan, V.; Gnanaraj, J.; Madhavi, S.; Liu, H. K. Lithium-Ion Conducting Electrolyte Salts for Lithium Batteries. *Chem.—Eur. J.* **2011**, *17*, 14326−14346.

(25) Antoniotti, S.; Dalla, V.; Duñach, E. Metal Triflimidates: Better than Metal Triflates as Catalysts in Organic Synthesis—The Effect of a Highly Delocalized Counteranion. *Angew. Chem., Int. Ed.* **2010**, *49*, 7860−7888.

(26) Klikovits, N.; Knaack, P.; Bomze, D.; Krossing, I.; Liska, R. Novel photoacid generators for cationic photopolymerization. *Polym. Chem.* **2017**, *8*, 4414−4421.

(27) Zhou, J.; Lancaster, S. J.; Walker, D. A.; Beck, S.; Thornton-Pett, M.; Bochmann, M. Synthesis, structures, and reactivity of weakly coordinating anions with delocalized borate structure: the assessment of anion effects in metallocene polymerization catalysts. *J. Am. Chem. Soc.* **2001**, *123*, 223−237.

(28) Castellanos, F.; Cavezzan, J.; Fouassier, J.-P.Onium Borates/Borates of Organometallic Complexes and Cationic Initiaton of Polymerization therewith. U.S. Patent 5,668,192 A, 1993; pp 4−5.

(29) Menczel, J. D.; Prime, R. B.*Thermal Analysis of Polymers: Fundamentals and Applications*; Wiley: Hoboken, NJ, USA, 2014; Chapter 2.

(30) Flory, P. J.*Principles of Polymer Chemistry*; Cornell University Press: Munich, 1953.
(31) Knaack, P.; Klikovits, N.; Tran, A. D.; Bomze, D.; Liska, R. Radical induced cationic frontal polymerization in thin layers. *J. Polym. Sci., Part A: Polym. Chem.* **2019**, *57*, 1155−1159.
(32) Castellanos, F.; Fouassier, J. P.; Priou, C.; Cavezzan, J. Synthesis, reactivity, and properties of new diaryliodonium salts as photoinitiators for the cationic polymerization of epoxy silicones. *J. Appl. Polym. Sci.* **1996**, *60*, 705−713.
(33) Cross, D. J.; Kenny, J. A.; Houson, I.; Campbell, L.; Walsgrove, T.; Wills, M. Rhodium versus ruthenium: contrasting behaviour in the asymmetric transfer hydrogenation of alpha-substituted acetophenones. *Tetrahedron: Asymmetry* **2001**, *12*, 1801−1806.
(34) Fischer, M.; Schmidtmann, M. B (C 6 F 5) 3-and HB (C 6 F 5) 2-mediated transformations of isothiocyanates. *Chem. Commun.* **2020**, *56*, 6205−6208.
(35) Herzig, T.; Schreiner, C.; Gerhard, D.; Wasserscheid, P.; Gores, H. J. Characterisation and properties of new ionic liquids with the difluoromono[1,2-oxalato(2-)-O,O′]borate anion. *J. Fluorine Chem.* **2007**, *128*, 612−618.
(36) Zugmann, S.; Moosbauer, D.; Amereller, M.; Schreiner, C.; Wudy, F.; Schmitz, R.; Schmitz, R.; Isken, P.; Dippel, C.; Müller, R.; Kunze, M.; Lex-Balducci, A.; Winter, M.; Gores, H. J. Electrochemical characterizaiton of electrolytes for lithium-ion batteries based on lithium difluoromono(oxalato)borate. *J. Power Sources* **2011**, *196*, 1417−1424.
(37) Lischka, U.; Wietelmann, U.; Marion, W.Lithium-bisoxalatoborat, Verfahren zu dessen Hersetllung und dessen Verwendung. DE 19829030 C1, 1999; p 4.
(38) Xia, L.; Lee, S.; Jiang, Y.; Xia, Y.; Chen, G. Z.; Liu, Z. Fluorinated electrolytes for li-ion batteries: The lithium difluoro (oxalato) borate additive for stabilizing the solid electrolyte interphase. *ACS Omega* **2017**, *2*, 8741−8750.
(39) Zhang, S.; Xu, C.; Jow, T. R.Metal borate synthesis process. U.S. Patent 7,820,323 B1, 2010.
(40) Ping, Q.; Xu, B.; Ma, X.; Tian, J.; Wang, B. An iron oxyborate Fe 3 BO 5 material as a high-performance anode for lithium-ion and sodium-ion batteries. *Dalton Trans.* **2019**, *48*, 5741−5748.
(41) Li, A.; Xu, L.; Li, S.; He, Y.; Zhang, R.; Zhai, Y. One-dimensional manganese borate hydroxide nanorods and the corresponding manganese oxyborate nanorods as promising anodes for lithium ion batteries. *Nano Res.* **2015**, *8*, 554−565.
(42) Kaliner, M.; Rupp, A.; Krossing, I.; Strassner, T. Tunable Aryl Alkyl Ionic Liquids with Weakly Coordinating Tetrakis ((1, 1, 1, 3, 3, 3-hexafluoropropan-2-yl) oxy) borate [B (hfip) 4] Anions. *Chem.—Eur. J.* **2016**, *22*, 10044−10049.
(43) Klikovits, N.; Sinawehl, L.; Knaack, P.; Koch, T.; Stampfl, J.; Gorsche, C.; Liska, R. UV-Induced Cationic Ring-Opening Polymerization of 2-Oxazolines for Hot Lithography. *ACS Macro Lett.* **2020**, *9*, 546−551.
(44) Mete, Y.; Knaack, P.; Liska, R. A systematic study of temperature-dependent cationic photopolymerization of cyclic esters. *Polym. Int.* **2022**, *71*, 797−803.
(45) Green, W. A.Sensitization and Synergy. *Industrial Photoinitiators: A Technical Guide*; Taylor & Francis: Boca Raton, 2010; Chapter 5.4, p 128.
(46) Taschner, R.; Knaack, P.; Liska, R. Bismuthonium- and pyrylium-based radical induced cationic frontal polymerization of epoxides. *J. Polym. Sci.* **2021**, *59*, 1841−1854.

https://doi.org/10.1021/acsapm.2c01465
ACS Appl. Polym. Mater. 2022, 4, 7878−7890